Experimental Investigation of Size Effects on the Thermal Conductivity of Silicon-Germanium Alloy Thin Films

Ramez Cheaito,[1] John C. Duda,[1,2] Thomas E. Beechem,[2] Khalid Hattar,[2] Jon F. Ihlefeld,[2] Douglas L. Medlin,[3] Mark A. Rodriguez,[2] Michael J. Campion,[2,4] Edward S. Piekos,[2] and Patrick E. Hopkins[1,*]

[1]*Department of Mechanical and Aerospace Engineering, University of Virginia, Charlottesville, Virginia 22904, USA*
[2]*Sandia National Laboratories, Albuquerque, New Mexico 87123, USA*
[3]*Sandia National Laboratories, Livermore, California 94550, USA*
[4]*Massachusetts Institute of Technology, Department of Material Science and Engineering, Cambridge, Massachusetts 02139, USA*

(Received 1 June 2012; published 8 November 2012)

We experimentally investigate the role of size effects and boundary scattering on the thermal conductivity of silicon-germanium alloys. The thermal conductivities of a series of epitaxially grown $Si_{1-x}Ge_x$ thin films with varying thicknesses and compositions were measured with time-domain thermoreflectance. The resulting conductivities are found to be 3 to 5 times less than bulk values and vary strongly with film thickness. By examining these measured thermal conductivities in the context of a previously established model, it is shown that long wavelength phonons, known to be the dominant heat carriers in alloy films, are strongly scattered by the film boundaries, thereby inducing the observed reductions in heat transport. These results are then generalized to silicon-germanium systems of various thicknesses and compositions; we find that the thermal conductivities of $Si_{1-x}Ge_x$ superlattices are ultimately limited by finite size effects and sample size rather than periodicity or alloying. This demonstrates the strong influence of sample size in alloyed nanosystems. Therefore, if a comparison is to be made between the thermal conductivities of superlattices and alloys, the total sample thicknesses of each must be considered.

DOI: 10.1103/PhysRevLett.109.195901 PACS numbers: 65.40.−b, 63.22.−m, 63.50.Gh, 68.37.−d

Silicon-germanium structures continue to be the focus of tremendous investment due to their widespread integration in thermoelectric power generation, optoelectronic devices, and high-mobility transistors. For example, bulk $Si_{1-x}Ge_x$ is an established high temperature thermoelectric material demonstrating a figure of merit, ZT, approaching unity at ≈ 1100 K [1]. Moreover, there has been much interest in engineering silicon-germanium systems for high ZT thermoelectrics by the manipulation of thermal properties via interface scattering effects. For these reasons, the thermal properties of $Si_{1-x}Ge_x$ systems have been studied extensively in a variety of material forms including superlattices of different period lengths [2–6], alloy-based superlattices [7,8], superlattice nanowires [9], doped $Si_{1-x}Ge_x$ superlattices and bulk alloys [5,10,11], and nanostructured bulk alloys [12]. These investigations have been accompanied with theoretical studies that have elucidated the underlying nature of phonon transport in these systems [10,13–16]. Most previous works allude to the fact that $Si_{1-x}Ge_x$-based superlattice structures exhibit thermal conductivities lower than the so-called alloy limit. These superlattices are often compared to SiGe alloy samples of much larger thicknesses. This neglects the potential size effects associated with the finite sample thicknesses of alloys and total sample thickness of superlattices, a fact that is often overlooked due to the assumption of strong phonon scattering at alloy sites. Here, in contrast, we show that these size effects associated with total sample size must be considered in the analysis and comparison of alloys and superlattices.

This idea is reinforced by recent computational and theoretical investigations into thermal conductivity of nanostructured $Si_{1-x}Ge_x$ systems. For example, when implementing nonequilibrium molecular dynamics simulations, Landry and McGaughey [17] found that the calculated values of thermal conductivity of a $Si_{0.5}Ge_{0.5}$ alloy were strongly dependent on the size of the simulation cell (more so than in a homogeneous Si domain [18]). Also via nonequilibrium molecular dynamics, Chen, Zhang, and Li [19] found that the thermal conductivities of Stillinger-Weber–type $Si_{1-x}Ge_x$ nanowires were substantially below those values obtained by Skye and Schelling [20], where the Green-Kubo approach was used to predict the thermal conductivities of bulk $Si_{1-x}Ge_x$ alloys. Finally, Garg *et al.* [21] used density functional perturbation theory to study the spectral dependence of thermal conductivity in $Si_{1-x}Ge_x$ alloys and found that more than half of the heat-carrying phonons had mean-free paths greater than 1 μm.

Whereas copious effort has been invested in quantifying the thermal conductivity of more complex nanostructured $Si_{1-x}Ge_x$ systems (i.e., superlattices, nanowires, etc.), there are far fewer reports that focused on experimentally investigating $Si_{1-x}Ge_x$ thin-film alloy thermal transport [2,6,7,22,23]. In response, we measure the thermal conductivity of thin-film $Si_{1-x}Ge_x$ alloys with thicknesses ranging from 39 to 427 nm along with different alloy

TABLE I. Thickness and alloy composition of the thickness and composition series samples.

	Thickness (nm)	Ge content (%)	κ(W m^{-1} K^{-1})
Thickness series	39 ± 0.9	20.0	1.83 ± 0.09
	88 ± 1.8	20.0	2.17 ± 0.10
	202 ± 2.1	20.0	2.69 ± 0.10
	427 ± 2.1	20.0	2.84 ± 0.18
Composition series	88 ± 1.8	20.0	2.17 ± 0.10
	135 ± 10.4	34.5	1.68 ± 0.30
	126 ± 10.1	45.0	1.79 ± 0.39

compositions over a temperature range of 141–300 K via time-domain thermoreflectance (TDTR). Significant reductions in the thermal conductivities of the thin films are observed as compared to their bulk counterparts. This reduction is attributed to boundary scattering of the long wavelength phonons, which serve as the primary thermal carriers. This result illuminates the substantial role of size effects on phonon transport in nondilute alloys and superlattices while diminishing the often-thought dominance of alloy scattering in thin-film alloys.

Two sample sets, as listed in Table I, were prepared: a thickness series with nominal composition $Si_{0.8}Ge_{0.2}$ and a composition series of slightly varying thicknesses. The samples were epitaxially grown by using metal-organic chemical vapor deposition on 100 mm diameter (001)-oriented single-crystalline silicon substrates. Substrate growth temperatures ranged between 650 and 700 °C. Sample thicknesses were verified by x-ray reflectivity and cross sectional transmission electron microscopy (TEM). Film stoichiometry was verified by Rutherford backscattering spectroscopy. Surface roughnesses were characterized by atomic force microscopy. In general, this level of characterization is necessary to minimize the uncertainty in the analysis of TDTR data.

We also assessed the defect densities within the films by TEM. These observations were conducted on plan-view specimens back-thinned from the silicon side by mechanical grinding and dimpling, followed by Ar + ion milling. Figure 1 shows TEM images from the plan-view specimens collected from the thickness series of $Si_{1-x}Ge_x$ films. As seen in the micrographs, the dislocation density increases with the film thickness. Therefore, if dislocations were to cause a reduction in thermal conductivity, the conductivity of the thickest samples would be the lowest. We will show that this is not the case.

We measure the thermal conductivities of the samples with TDTR [24,25] utilizing a double color pump-probe setup. The details of our TDTR systems and the measurement method are detailed elsewhere [24,26,27]. For two selected samples, the temperature-dependent thermal conductivities are measured from 141 to 300 K by using a liquid nitrogen cryostat with optical access.

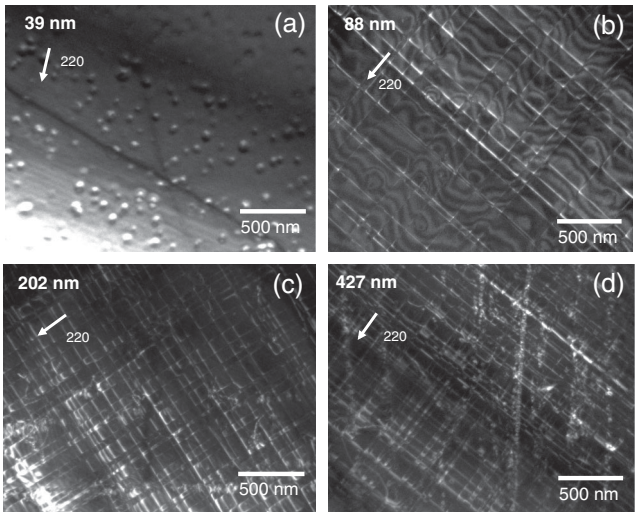

FIG. 1. Plan-view TEM images showing increasing density of dislocations with increasing film thickness. Images were collected under weak-beam dark-field conditions using a {220}-type diffracting vector.

For TDTR transduction, the $Si_{1-x}Ge_x$ samples were coated with aluminum via *e*-beam evaporation prior to TDTR testing. The aluminum thickness is locally confirmed by picosecond acoustics [28,29]. The thermal conductivity of the silicon substrate is measured separately by using a reference Si sample from the same lot as the substrate. We assume literature values for Al film and Si substrate heat capacities. Temperature-dependent heat capacity values for $Si_{1-x}Ge_x$ were taken from Ref. [30]. At least four measurements were taken on each sample at different locations to ensure relative uniformity. We also measured repeats of selected samples to confirm that obtained results are not just associated with a particular batch of samples. Mean values for the resulting thermal conductivities for each of the films are listed in Table I and plotted in Figs. 2 and 3. The uncertainty in thermal conductivity values shown in Table I accounts for the uncertainty in $Si_{1-x}Ge_x$ film thickness, uncertainty in aluminum thickness, and the standard deviation about the mean of the measurements performed on each sample.

Figure 2(a) compares the measurement results to those acquired on various $Si_{1-x}Ge_x$ structures reported previously [2,4,6–8,23]. These values are plotted against either period length, in the case of a superlattice, or thickness in the case of a thin-film alloy. Similarly, in Fig. 2(b), the same data are plotted versus the total thickness of the sample for both superlattices and alloy films. A clearer trend in the thermal conductivities is observed when compared against the total sample thickness [Fig. 2(b)] as opposed to the superlattice period [Fig. 2(a)]. This suggests that the total film thickness rather than periodicity is inhibiting the thermal transport in both superlattices and alloy films. The measured alloy films show a thermal conductivity 3–5 times lower than bulk. Since the thermal

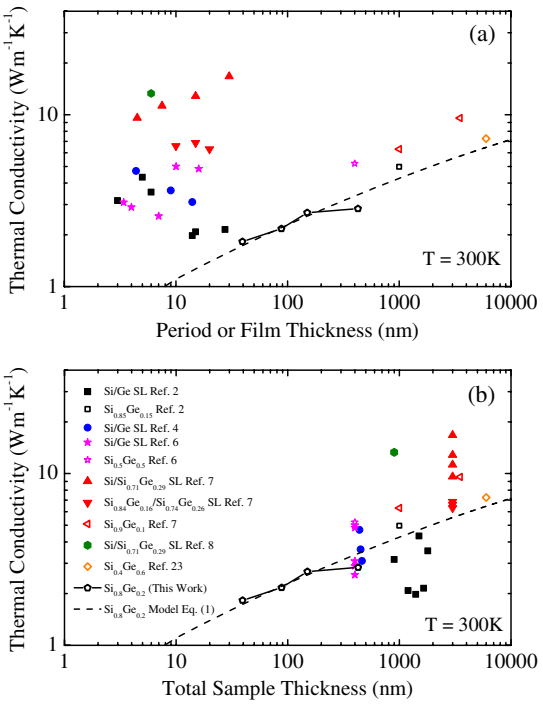

FIG. 2 (color online). Thermal conductivity measurements on $Si_{0.8}Ge_{0.2}$ of the thickness series along with previously reported values of different Si/Ge superlattices, alloy-based superlattices, and alloy films at room temperature. Closed symbols represent superlattices; open symbols represent $Si_{1-x}Ge_x$ films. The thermal conductivity is plotted versus (a) period or film thickness and (b) total sample thickness. The figure also shows the model presented in Eq. (1).

conductivity increases with thickness, we can safely say that the reduction is not due to film dislocations. Intriguingly, the thermal conductivities of the alloy thin films measured in this Letter are among the lowest of any of the previous measurements on SiGe-based thin-film systems. We note that the only previous data that approach our lowest measured value are those in which the authors admit that the measured samples have poor crystal quality (black filled squares in Fig. 2) [2].

To quantify this effect, we turn to a model originally proposed by Wang and Mingo [31], in which thermal conductivity κ is given by

$$\kappa = \int_0^{\hbar\omega_c/k_B T} \frac{k_B^4 T^3}{2\pi^2 v\hbar^3} \tau(T,y) y^4 \frac{\exp(y)}{[\exp(y)-1]^2} dy, \quad (1)$$

where k_B is Boltzmann's constant, $\hbar$ is Planck's constant divided by 2π, T is temperature, and $y = \hbar\omega/k_B T$ is a dimensionless parameter. The average velocity v is calculated by $v = [(1-x)v_{Si}^{-2} + xv_{Ge}^{-2}]^{-1/2}$, where x is the Ge concentration and v_{Si} and v_{Ge} are the average speeds of sound in Si and Ge, respectively, as calculated by Wang and Mingo [31]. The scattering time for a given frequency, τ, is related to the individual processes via Mattheissen's rule $\tau = (\tau_U^{-1} + \tau_a^{-1} + \tau_b^{-1})^{-1}$, where τ_U, τ_a, and τ_b are the umklapp, alloy, and boundary scattering times, respectively. These are given by

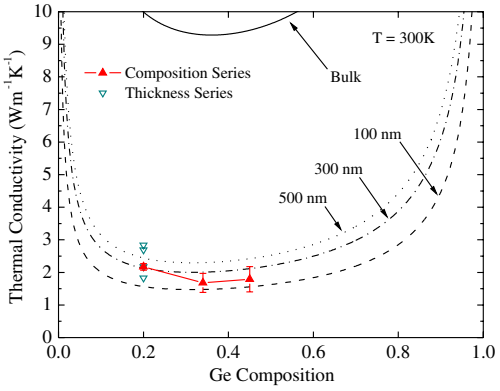

FIG. 3 (color online). Predictions of the thermal conductivity as a function of Ge composition for bulk and thin-film $Si_{1-x}Ge_x$ of three different thicknesses calculated at room temperature by using Eq. (1). The symbols correspond to experimental data on the thickness series (down open triangles) and composition series (up filled triangles). With decreasing film thickness, alloying induces smaller and smaller changes in the thermal conductivity as size effects begin to dominate.

$$\tau_U = [(1-x)\tau_{U,Si}^{-1} + x\tau_{U,Ge}^{-1}]^{-1}, \quad (2)$$

$$\tau_a = [x(1-x)A\omega^4]^{-1}, \quad (3)$$

and

$$\tau_b = d/v, \quad (4)$$

where

$$\tau_{U,Si(Ge)}^{-1} = B_{Si(Ge)}\omega^2 \exp(-C_{Si(Ge)}/T). \quad (5)$$

The constants A, B, and C are taken from Ref. [31], and d is the film thickness.

Our model is thus identical to that in Ref. [31] except for the cutoff frequency, which we define as $\omega_c = 2\pi v/a$, with a being the lattice constant of the $Si_{1-x}Ge_x$ film approximated by Vegard's law: $a = (1-x)a_{Si} + xa_{Ge}$, where a_{Si} and a_{Ge} are the lattice constants of silicon and germanium, respectively. Equation (1) assumes a dispersionless, Debye system. This is acceptable for $Si_{1-x}Ge_x$ systems with nondilute alloying compositions, since the dispersive phonons scatter strongly with the alloy atoms due to their high frequencies. This assertion is substantiated by the reasonable agreement found between this model, our data, and previously reported measurements on thin-film alloys in Refs. [2,7,23] as shown in Fig. 2.

To first assess the role of alloy composition, Fig. 3 shows the measured thermal conductivity versus Ge concentration and the predictions of the thermal conductivity for bulk and thin-film $Si_{1-x}Ge_x$ of three different thicknesses at room temperature using Eq. (1). For $Si_{1-x}Ge_x$ with $0.2 < x < 0.8$, we found that the thermal conductivity is almost flat and in agreement with our experimental results. This lack of dependence on the Ge concentration is much more pronounced in thin films than

in bulk materials, suggesting that size effects more significantly influence the transport in $Si_{1-x}Ge_x$ films than does alloying when $0.2 < x < 0.8$. This is further supported in Fig. 3, where changes in thickness from 39 to 427 nm are found to have a much greater effect on the thermal conductivity than variations in Ge content. Last, this trend is consistent with the previous computational work of Chen, Zhang, and Li [19], where the thermal conductivities of Stillinger-Weber–type $Si_{1-x}Ge_x$ nanowires were relatively insensitive to changes in composition for $0.2 < x < 0.8$.

To understand the degree to which the different scattering processes affect thermal conductivity, we analyze the spectral contribution to thermal conductivity by calculating the integrand of Eq. (1). Figure 4 shows the spectral thermal conductivity for the 427 and 39 nm films having a Ge content of 20%. The spectral curve increases with frequency reaching a peak at around 10 and 18 Trad s^{-1} for the 427 and 39 nm films, respectively, and decreases thereafter. This demonstrates that low frequency (long wavelength) phonons more significantly contribute to the transport and thus the treatment of alloys as a dispersionless (i.e., Debye-like) system is valid. The inset reveals that, in this low frequency regime, boundary scattering is the dominant process, since the boundary scattering time (τ_b) is shortest for the modes carrying the most heat. It is only at high frequencies that alloy scattering is the limiting mechanism. As a result, we conclude that the low thermal conductivities of $Si_{1-x}Ge_x$ alloy thin films arise primarily due to the boundary scattering in the film rather than the effects of the alloying in the material.

This interpretation is further demonstrated through an examination of temperature dependence of the thermal conductivity presented in Fig. 5. The 427 and 202 nm $Si_{0.8}Ge_{0.2}$ films exhibit reasonable agreement with our model over a range of 141–300 K. We also plot temperature-dependent thermal conductivity of a Si/Ge superlattice of 462 nm total thickness from Ref [4]. Moreover, we plot our model assuming the thickness and average composition of the superlattice in Fig. 5. The agreement between the superlattice data,

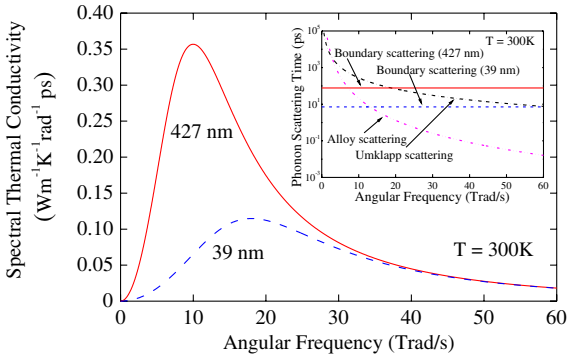

FIG. 4 (color online). Spectral thermal conductivity for the 427 and 39 nm $Si_{0.8}Ge_{0.2}$ films at room temperature. The inset shows the alloy, umklapp, and the boundary scattering times versus angular frequency for the 427 and 39 nm films.

our 427 nm $Si_{0.8}Ge_{0.2}$ film, and a $Si_{0.5}Ge_{0.5}$ alloy model of the same superlattice total thickness (462 nm) further suggests the existence of similar phonon scattering mechanisms that contribute to the thermal conductivity based on the overall sample size. In addition, we plot the thermal conductivities of amorphous silicon [2], bulk $Si_{0.8}Ge_{0.2}$ alloy [2], dilute alloys with 0.13%, 0.25%, and 1.0% Ge compositions [32], and bulk Si [33]. The thermal conductivities of the $Si_{1-x}Ge_x$ films and Si/Ge superlattice have similar temperature trends to that of amorphous Si and the bulk $Si_{1-x}Ge_x$ alloy, indicating the strong effect of alloy scattering over this temperature range. The reduction of thermal conductivity in the alloy film and superlattice compared to the bulk alloy is attributed to the additional scattering mechanisms of long wavelength phonons with the sample boundaries, as discussed throughout this Letter. In this regime, the thermal conductivity of bulk Si and dilute SiGe alloys show a clear trend indicative of umklapp scattering ($\kappa \propto 1/T$). This umklapp behavior is absent in nondilute alloyed systems. This further alludes to the fact that alloy scattering is the dominant high frequency phonon scattering mechanism over this temperature range, whereas boundary scattering is affecting the low frequency phonons in these nanosystems. This is further analyzed in our discussion and analysis pertaining to Fig. 4.

In conclusion, we have shown that the reductions in thermal conductivity in silicon-germanium alloy thin films

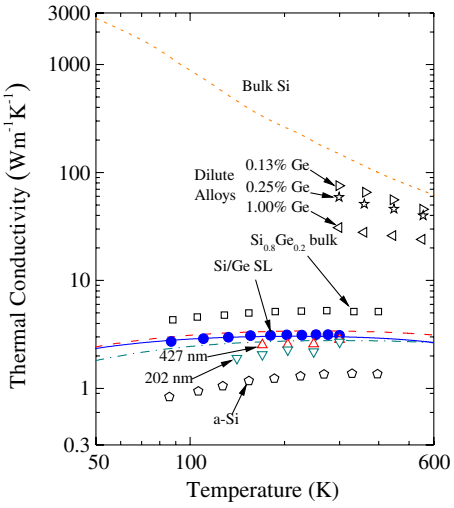

FIG. 5 (color online). Thermal conductivity of various SiGe and Si systems. Symbols represent our data on 427 nm $Si_{0.8}Ge_{0.2}$ (up open triangles) and 202 nm $Si_{0.8}Ge_{0.2}$ (down open triangles), Si/Ge SL of 14 nm period thickness and 462 nm total thickness (filled circles) from Ref. [4], bulk $Si_{0.8}Ge_{0.2}$ (open squares) from Ref. [2], amorphous Si (open pentagons) also from Ref. [2], and dilute alloy films of 0.13% (right open triangles), 0.25% (open stars), and 1% (left open triangles) Ge concentrations from Ref. [32]. Lines correspond to predictions of the model presented in Eq. (1) for 427 nm $Si_{0.8}Ge_{0.2}$ film (dashed line), 202 nm $Si_{0.8}Ge_{0.2}$ (dash-dotted line), and 462 nm $Si_{0.5}Ge_{0.5}$ (solid line) and bulk Si (dotted line) from Ref. [33].

are ascribed to the finite sizes of the samples. For thin-film alloys and superlattices, the boundary conditions of the samples must be considered when comparing the thermal conductivity to the alloy limit. That is, if an honest comparison is to be made between the thermal conductivities of superlattices and alloys, the total sample thickness of each must be considered. In the case of superlattices, further study is necessitated in terms of understanding the interplay between the effect of period thickness and total sample thickness on the thermal conductivity.

This work was performed in part at the Center for Atomic, Molecular, and Optical Science (CAMOS) at the University of Virginia. We are appreciative of funding through the Laboratory Directed Research and Development program at Sandia National Laboratories. Sandia National Laboratories is a multiprogram laboratory managed and operated by Sandia Corporation, a wholly owned subsidiary of Lockheed Martin Corporation, for the U.S. Department of Energy National Nuclear Security Administration under Contract No. DE-AC04-94AL85000. P. E. H. and J. C. D are appreciative for support from NSF Grant No. CBET 1134311.

*phopkins@virginia.edu

[1] G. J. Snyder and E. S. Toberer, Nature Mater. **7**, 105 (2008).
[2] S.-M. Lee, D. G. Cahill, and R. Venkatasubramanian, Appl. Phys. Lett. **70**, 2957 (1997).
[3] R. Venkatasubramanian, E. Siivola, and T. Colpitts, in *Proceedings of the Seventeenth International Conference on Thermoelectrics* (IEEE, New York, 1998), p. 191, http://ieeexplore.ieee.org/xpls/abs_all.jsp?arnumber=740350.
[4] T. Borca-Tasciuc, W. Liu, J. Liu, T. Zeng, D. W. Song, C. D. Moore, G. Chen, K. L. Wang, and M. S. Goorsky, in *Proceedings of the Eighteenth International Conference on Thermoelectrics* (IEEE, New York, 1999), p. 201, http://ieeexplore.ieee.org/xpl/articleDetails.jsp?reload=true&arnumber=843368&content=Conference+Publications.
[5] T. Borca-Tasciuc, W. Liu, J. Liu, T. Zeng, D. W. Song, C. D. Moore, G. Chen, K. L. Wang, M. S. Goorsky, T. Radetic, R. Gronsky, T. Koga, and M. S. Dresselhaus, Superlattices Microstruct. **28**, 199 (2000).
[6] S. Chakraborty, C. A. Kleint, A. Heinrich, C. M. Schneider, J. Schumann, M. Falke, and S. Teichert, Appl. Phys. Lett. **83**, 4184 (2003).
[7] S. T. Huxtable, A. R. Abramson, C.-L. Tien, A. Majumdar, C. LaBounty, X. Fan, G. Zeng, J. E. Bowers, A. Shakouri, and E. T. Croke, Appl. Phys. Lett. **80**, 1737 (2002).
[8] G. Chen, S. Q. Zhou, D.-Y. Yao, C. J. Kim, X. Y. Zheng, Z. L. Liu, K. L. Wang, X. Sun, and M. S. Dresselhaus, in *Proceedings of the Seventeenth International Conference on Thermoelectrics* (IEEE, New York, 1998), p. 202, http://ieeexplore.ieee.org/xpls/abs_all.jsp?arnumber=740352.
[9] D. Li, Y. Wu, R. Fan, P. Yang, and A. Majumdar, Appl. Phys. Lett. **83**, 3186 (2003).
[10] C. B. Vining, J. Appl. Phys. **69**, 331 (1991).
[11] G. Joshi, H. Lee, Y. Lan, X. Wang, G. Zhu, D. Wang, R. W. Gould, D. C. Cuff, M. Y. Tang, M. S. Dresselhaus, G. Chen, and Z. Ren, Nano Lett. **8**, 4670 (2008).
[12] X. W. Wang, H. Lee, Y. C. Lan, G. H. Zhu, G. Joshi, D. Z. Wang, J. Yang, A. J. Muto, M. Y. Tang, J. Klatsky, S. Song, M. S. Dresselhaus, G. Chen, and Z. F. Ren, Appl. Phys. Lett. **93**, 193121 (2008).
[13] G. A. Slack and M. A. Hussain, J. Appl. Phys. **70**, 2694 (1991).
[14] G. Chen and M. Neagu, Appl. Phys. Lett. **71**, 2761 (1997).
[15] A. A. Kiselev, K. W. Kim, and M. A. Stroscio, Phys. Rev. B **62**, 6896 (2000).
[16] S. Volz, J. B. Saulnier, G. Chen, and P. Beauchamp, Microelectron. J. **31**, 815 (2000).
[17] E. S. Landry and A. J. H. McGaughey, Phys. Rev. B **79**, 075316 (2009).
[18] D. P. Sellan, E. S. Landry, J. E. Turney, A. J. H. McGaughey, and C. H. Amon, Phys. Rev. B **81**, 214305 (2010).
[19] J. Chen, G. Zhang, and B. Li, Appl. Phys. Lett. **95**, 073117 (2009).
[20] A. Skye and P. K. Schelling, J. Appl. Phys. **103**, 113524 (2008).
[21] J. Garg, N. Bonini, B. Kozinsky, and N. Marzari, Phys. Rev. Lett. **106**, 045901 (2011).
[22] D. G. Cahill, A. Bullen, and S.-M. Lee, High Temp. High Press. **32**, 135 (2000).
[23] Y. K. Koh and D. G. Cahill, Phys. Rev. B **76**, 075207 (2007).
[24] P. E. Hopkins, J. R. Serrano, L. M. Phinney, S. P. Kearney, T. W. Grasser, and C. T. Harris, J. Heat Transfer **132**, 081302 (2010).
[25] D. G. Cahill, K. Goodson, and A. Majumdar, J. Heat Transfer **124**, 223 (2002).
[26] A. J. Schmidt, X. Chen, and G. Chen, Rev. Sci. Instrum. **79**, 114902 (2008).
[27] D. G. Cahill, Rev. Sci. Instrum. **75**, 5119 (2004).
[28] C. Thomsen, J. Strait, Z. Vardeny, H. J. Maris, J. Tauc, and J. J. Hauser, Phys. Rev. Lett. **53**, 989 (1984).
[29] C. Thomsen, H. T. Grahn, H. J. Maris, and J. Tauc, Phys. Rev. B **34**, 4129 (1986).
[30] H.-M. Kagaya, Y. Kitani, and T. Soma, Solid State Commun. **58**, 399 (1986).
[31] Z. Wang and N. Mingo, Appl. Phys. Lett. **97**, 101903 (2010).
[32] D. G. Cahill, F. Watanabe, A. Rockett, and C. B. Vining, Phys. Rev. B **71**, 235202 (2005).
[33] C. Y. Ho, R. W. Powell, and P. E. Liley, J. Phys. Chem. Ref. Data **1**, 279 (1972).